END
DATE
FILMED
10-81
DTIC

AFGL - TR - 81 - 0137

GEOKINETIC ENVIRONMENT INVESTIGATIONS

Eugene B. Hartnett
Eric D. Carleen
Joseph I. Blaney

Weston Observatory
Department of Geology and Geophysics
Boston College
381 Concord Rd.
Weston, Massachusetts

31 March 1981

Final Report for period 1 October 1977 - 30 September 1980

DTIC
SELECTE
SEP 10 1981

D

REPORT DOCUMENTATION PAGE	READ INSTRUCTIONS BEFORE COMPLETING FORM

1. REPORT NUMBER	2. GOVT ACCESSION NO.	3. RECIPIENT'S CATALOG NUMBER
AFGL-TR-81-0137	AD-A104 048	

4. TITLE (and Subtitle)	5. TYPE OF REPORT & PERIOD COVERED
GEOKINETIC ENVIRONMENT INVESTIGATIONS	Final Report 1 Oct 1977 — 30 Sep 1980
	6. PERFORMING ORG. REPORT NUMBER

7. AUTHOR(s)	8. CONTRACT OR GRANT NUMBER(s)
Eugene B. Hartnett Eric D. Carleen Joseph I. Blaney	F19628-78-C-0008

9. PERFORMING ORGANIZATION NAME AND ADDRESS	10. PROGRAM ELEMENT, PROJECT, TASK AREA & WORK UNIT NUMBERS
Weston Observatory, Boston College Department of Geology and Geophysics Weston, Massachusetts 02193	62101F 760009AA

11. CONTROLLING OFFICE NAME AND ADDRESS	12. REPORT DATE
Air Force Geophysics Laboratory Hanscom Air Force Base, Massachusetts 01731 Manager/ Henry A. Ossing/ LWH	31 Mar 1981
	13. NUMBER OF PAGES
	63

14. MONITORING AGENCY NAME & ADDRESS(if different from Controlling Office)	15. SECURITY CLASS. (of this report)
	unclassified
	15a. DECLASSIFICATION/DOWNGRADING SCHEDULE

16. DISTRIBUTION STATEMENT (of this Report)

Approved for public release; distribution unlimited

17. DISTRIBUTION STATEMENT (of the abstract entered in Block 20, if different from Report)

18. SUPPLEMENTARY NOTES

19. KEY WORDS (Continue on reverse side if necessary and identify by block number)

Geokinetics	Rocket Plume Acoustics
Seismicity	Power Spectra Density
Motion Spectra	Least Squares Fit
Source Characteristics	Azimuth Transfer

20. ABSTRACT (Continue on reverse side if necessary and identify by block number)

This report covers the development and implementation of special concepts, techniques and instrumentation for the collection, analysis and application of geokinetic data. The Geokinetic Data Acquisition System (GDAS) was modified, maintained and operationally deployed to various sites designated by AFGL. Tests were conducted at the Defense Nuclear Agency (DNA) CASINO Facility in Maryland; Central Inertial Guidance Test Facility (CIGTF), Holloman AFB, N.M.;

DD FORM 1473 EDITION OF 1 NOV 65 IS OBSOLETE
1 JAN 73

Block 20   Continued

Space Transportation System (STS) Launch Complex, Vandenberg AFB,
CA. and the SAC Wing V Minuteman Complex at Cheyenne, Wy.

The CASINO data contributed to SAMSO's MX/TGG Advanced Develop-
ment Bridge II Program for radiation hardening of third generation
hardware.   The CIGTF investigation supported USAF requirements for
highly precise azimuth references.   The Hill AFB
the performance of a minuteman III missile guidance system in an
engineering silo.   The STS program at Vandenberg AFB was to assist
in determining the nature of a Titan III-D pressure load.   The SAC
Wing V deployment was to investigate plateau/valley basin geologic
characteristics in respect to motion response.

The most important aspect of this work was the upgrade of the
GDAS for the timely accumulation and reduction of field data for;
(1) engineering analysis and interpretation, (2) upgrading geokinetic
data reduction formatting techniques, (3) development and applica-
tion of theoretical model studies correlating geokinetic data with
areal geology and its impact on local Air Force facilities and
weapons systems and (4), improve accuracy and reliability of the
GDAS.

Accession For	
NTIS GRA&I	X
DTIC TAB	☐
Unannounced	☐
Justification	
By	
Distribution/	
Availability Codes	
Dist	Avail and/or Special
A	

SUMMARY

The primary objectives of this research were to develop specialized technical expertise, and to apply original concepts to critical problems affecting strategic USAF weapons systems and facilities. Work was primarily carried out at the Boston College Weston Observatory, Weston, Massachusetts and at representative geographical locations specifically designated by the Air Force Geophysics Laboratory. The following tasks were of primary interest to the study:

Develop and prepare plans for implementing geokinetic investigations in support of the Space Transportation System test and operational firings, and potential MX siting locations. Monitor rocket and explosion firings for determining air/ ground impedance characteristics at Vandenberg AFB pertinent to facility design modifications.

Modify, maintain and field adapt the Geokinetic Data Acquisition System (GDAS) and the Automated Azimuth Measuring System (AAMS) to the collection, recovery and reduction of environmental motion data.

Analyze geokinetic field data in order to update existing collection and reduction techniques and prepare the data for engineering analyses and interpretation.

Develop and conduct theoretical model studies correlating geokinetic data with areal geology and establish its impact on local Air Force facilities and weapon systems.

Conduct an investigation of the motion environment within the Wing V Minuteman fleet at Cheyenne, Wyoming. Improve definition of near and far field seismic characteristics of an alluvial valley as it pertains to the BMO-MX program.

PREFACE

This research was performed by personnel of the Boston College Weston Observatory, Weston, Massachusetts. It was sponsored by the Air Force Geophysics Laboratory Terrestrial Sciences Division under Contract F19628-78-C-0008. The work was directed towards the expansion, refinement and implementation of conceptual and applied geokinetic environment theory and technology developed under previous AFGL contracts. Specific geographical areas and physical facilities, important to USAF operations and strategic capabilities, were studied and reported upon.

Tests were conducted at: Advanced Inertial Test Laboratory, Holloman AFB, New Mexico in conjunction with the Geodetic Survey Squadron: DNA CASINO Facility at Silver Spring, Maryland; Wing V, Cheyenne, Wyoming and at Vandenberg AFB, California.

Field data acquired at the Hill Engineering Test Facility at Ogden, Utah under the previous contract (F19628-76-C-0007) were subsequently analyzed and documented under the follow-on contract covered by this final report.

The authors of this report acknowledge the significant contributions of Mr. Carl Syverson and Mr. William Atwell during their employment under this contract. Their accomplishments are interspersed throughout the entire report.

We also thank Mrs. Joy O'Malley for her patience, advice and competence in preparing this report.

TABLE OF CONTENTS

1. INTRODUCTION - AUTOMATED AZIMUTH MEASURING SYSTEM (AAMS)

The AAMS is an automated inertial azimuth measuring
system designed to obtain highly accurate all-weather azimuth
measurements. The incorporation of tilt correction measure-
ments into AAMS improves the accuracy of azimuth data to per-
mit a precise motion history of azimuth at much higher frequen-
cies than traditional celestial azimuth determinations. Auto-
matic angle measurements using an autocollimator on a precise
indexing table enable azimuth transfers to multiple targets
without the introduction of human error.

The AAMS was further upgraded to increase its precision
and automation. Improvements included replacing noisy elec-
tronics with precision linear power packs, state of the art
optics and application of advanced tiltometry hardware and tech-
niques. Resident microcomputers and the latest microprocessor
technology were employed for automatic sequencing and on-line
signal processing. The flexibility of software control lends
itself to the continued optimization of AAMS operation, data
acquisition,and processing thereby fulfilling a wide variety
of Air Force needs for precise azimuth measurements.

An in-depth study of the special test module (STM)design
was made to improve the operational performance of the AAMS.
Substitution of external DC power supplies eliminated some of
the electrical noise on the STMs which influence gyrocompass ac-
curacy. Evaluation of the micro-radian autocollimator in sup-
port of AFGL analyses led to the introduction of an automatic
nulling circuit. This circuit uses the ouput signal of the
autocollimator to drive the inductosyn table servo loop to a
null condition on multiple mirror references. Logic and control
electronics were designed to integrate this automatic function
with the SERDEX controller. Continued improvement of the AAMS
was hindered because of inaccurate circuit schematics and num-
erous component failures with subsequent difficulties in

obtaining replacement parts.

A Bedford Computer Systems printer/plotter was purchased
and interfaced with the LSI – 11 microcomputer to give the AAMS
a real-time data plotting capability. Upgrading of the data
acquisition software program was accomplished:32 K of random-
access memory provided by AFGL was installed into the system
and a successful operational checkout demonstrated by acquiring
data from the two ALS units. Custom designed biaxial tilt sys-
tems purchased from Instech of Austin, Texas were installed in
the ALS geoceivers. Small DC solenoids had to be incorporated
on each tiltmeter to overcome the Y tilt component stiction
after geosensor azimuth slews. Autocollimator tests showed that
range requirements associated with forthcoming field trips could
not be met by any of the autocollimators on hand. As a result,
the Micro-Radian unit was returned to the manufacturer for an
upgrade to potentially achieve a capture range of 100 feet.

External power supplies with overvoltage protection for
each geosensor control indicator were installed. Temperature
sensors and their associated electronics were fabricated and
installed inside each geosensor. The availability of slip
rings did not require multiplexing the temperature signals as
previously anticipated. Additional analog line drivers, re-
covery amplifiers, and filters were installed to provide the
AAMS with a measurement capability for 26 analog sensors.
The AAMS system was interfaced to a second LSI-11 computer and
software was developed to provide a real-time analysis capabil-
ity.

The Automatic Azimuth Measuring System was deployed at
F.E. Warren AFB for calibration during Jan-Feb 1979 to obtain
useful tilt data. In order to make gyro tilt and tilt rate cor-
rections, a 15 second delay was successfully implemented in

the STM azimuth and rotational slew commands that follow the STM's sample interval. Software modifications in the data acquisition program were made to allow "autonulling" of the Inductosyn table. These modifications included a ten second autonulling period for the Inductosyn table to acquire a given mirror. A ten second interval followed for sampling the Inductosyn table while still in the autonull mode. Software efforts were directed towards the development of programs that filter the STM tiltmeter data during the sample period. Development of a LSI-11 executable multiple regression program was also initiated. Several runs of the ALS units on the Weston test pier showed standard deviations, in most cases, of less than one arcsecond (uncorrected azimuth). In an attempt to gain better understanding of tilt and temperature data inside the STM units, tilt and temperature data were collected at various locations on the tiltmeter and its mounting block. Numerous regressions were performed on the data with the results given to AFGL for further analysis. The AAMS data acquisition software was modified to sample the STM tiltmeters at two different sample rates. Modifications to real-time and tape plotting routines were necessary to process this tiltmeter data at differing rates.

1.1 STATE OF THE ART

The aerospace industry has traditionally relied upon stellar observations to determine the azimuths for precise geodetic references. However, astro-optical azimuth techniques have significant drawbacks. Typically, a large number of observations taken over a period of months to years are required to develop an accurate data base. Observations require optimum weather conditions in order to see the reference star. Field data must be reduced using star position catalogs, and then corrected for such effects as polar motion. Effects from such phenomenon as refraction due to the earth's atmosphere

are still uncertain.

Estimates of uncertainties associated with stellar azimuth measurements do appear to be quite small. However, these estimates can be misleading. Typically, an estimate of uncertainty is expressed as the standard error of the mean or of a "least squares" linear fit of the data. Thus, as the number of observations is increased, the estimate of the uncertainty will usually decrease. However, these statistical estimates do not account for the fact that most stellar azimuth observations are made at night. As a consequence, any motions of the azimuth reference device having periods shorter than 24 hours will not appear in the mathematical estimate of the azimuth uncertainty.

1.2 REQUIREMENT

Requirements for highly precise azimuth references for USAF weapons systems have led to an improved automated azimuth measuring system (AAMS). The AAMS represents the state-of-the art for a highly accurate, automated, all-weather azimuth capability which can be used in either a laboratory or specialized field environment. The present system consists of two integrated inertial sensors, an angle transfer system, a tiltmeter array and a microprocessor. The inertial sensors use gimbal-mounted rate gyrocompasses to indicate the azimuths of two transfer mirrors with respect to true North. The azimuths are transferred to any number of reflectors by an autocollimator on a precision indexing table. Sight tubes carry low velocity air along each optical path. Highly sensitive tiltmenters are used to measure and correct for errors due to base motions of the inertial sensors. Data handling and functional operation are controlled by the microprocessor. Recent results indicate a standard deviation of 2.1 arc seconds for a single observation.

1.3   INERTIAL AZIMUTH SYSTEMS

In recent years, numerous government and commercial agencies have been using inertial measurement systems for practical geodetic applications. These inertial azimuth systems have a number of advantages over traditional astro-optical methods for establishing azimuth references. They are not affected by such traditional restrictions as weather fluctuations, requirements for darkness during observation periods, human observation errors and errors associated with azimuth transfer from the outside astronomical reference to the desired indoor reference. A further advantage of inertial systems is the increased observation frequency which assures a more complete description of the higher frequency motions of the azimuth reference.

However, an inherent disadvantage of most inertial azimuth measuring systems is that they cannot distinguish between sensing earth rate and sensing rates due to tilt motions. Boston College, under AFGL sponsorship, has investigated the effects of tilt motions on inertial sensors and determined that the accuracy of inertial azimuth measurements can be significantly improved by measuring and correcting for the errors due to tilts and tilt rates. This principle is employed in the automated azimuth measuring system (AAMS). The system, described herein, was developed to meet the specialized requirements for the test and evaluation of Air Force weapons systems. It is especially suitable for use in indoor environments where highly accurate azimuth references are required and access to a stellar reference is restricted.

1.3.1   SYSTEM DESIGN

The AAMS is comprised of two service test model Azimuth Laying Sets (ALSs), which inertially determine azimuth; an

inductosyn/autocollimator azimuth transfer system; a tiltmeter
array and a microprocessor. A plastic enclosure with controlled
airflow is used to reduce thermal gradients near the AAMS, and
sight tubes with forced air are used between the AAMS and the
target to reduce refractive bending of the lines of sight.

1.3.2 AZIMUTH LAYING SETS

The ALSs are the primary azimuth measuring components of
the AAMS. Each ALS is comprised of a geosensor, which uses four-
position gyrocompassing to determine the orientation of its input
axis with respect to True North, and a control indicator, which
controls the operation of the geosensor and displays the input
axis misalignment from True North. The two ALSs are synchronized,
thereby providing two simultaneous azimuth estimates.

The primary component of the geosensor is the rate-sensing
gyrocompass. The gyro has three orthogonal axes - -spin, input
and output - - which are supported on two gimbals. A small
mirror is mounted approximately perpendicular to, and on each end
of the North-South gimbal for the purpose of azimuth transfer.
The gimbal arrangement allows for rotating and inverting the
gyrocompass into four orientations, thereby cancelling potential
systematic errors.

In a typical operational arrangement, the axes are align-
ed as follows: the spin axis (AS) is approximately north-south;
the input axis (IA) is approximately east-west; and the output
(OA) is up or down. Earth rate, sensed as a torque about the IA,
is balanced by a known torque applied about the OA. The value
of the balancing torque is proportional to the component of
earth rate acting upon the IA, thus providing a measure of the
orientation of the IA with respect to the earth's spin axis.

By aligning the IA as closely as possible to east or west, the
component of earth rate being sensed by the IA is minimized
(exactly east or west results in no torque about the IA) and
the sensitivity to small changes in input rate can be increased.
Accordingly, the system's azimuth resolution is increased as well.

The component of earth rate being sensed by the gyro-
compass is also a function of the cosine of the latitude of
operation. This latitude term is automatically incorporated in
the balancing loop by application of a variable voltage scale
factor to the balancing torque. The scale factor is determined
by calibrating a potentiometer setting on the ALS control in-
dicator while moving the alignment of the geosensor IA through
a known angle.

A single AAMS azimuth determination is referred to as a
"sequence". During any given AAMS sequence, earth rate is sam-
pled with the ALS gyrocompass alternately aligned into the four
positions of input axis east or west, and output axis up or down
to eliminate systematic errors. These four sample positions
are called "measurement positions". As the gyrocompass orienta-
tion is changed, the polarity of the torque about the input
axis due to earth rate is also changed. Thus, at the end of each
sequence the four samples are summed, and the result is display-
ed by the ALS. Except for a small bias error which is deter-
mined during calibration, this result represents the true azi-
muth of the ALS mirror normal as long as there has been no tilt
of the IA during the measurement position. However, this is
not normally the situation.

1.3.3 TILTMETERS

The earth rate component being sensed by the gyrocompass,
and therefore the azimuth estimate, is affected by tilt in two

ways. First, if the static tilt (i.e. level) of the gyrocompass
is changed, the component of the earth rate vector which acts on
the IA will also change. Second, the gyrocompass cannot dis-
tinguish between earthrate and tilt rates being sensed by its
IA. Thus, if the tilt of the IA varies during any measurement
position, the resulting tilt rates will be interpreted by the
gyrocompass as earth rate.

In its present configuration, tilt of the ALS geosensor
is measured by an array of orthogonal tiltmeters, and corrections
for tilt and tilt-rate effects are applied to the azimuth data.
Six Radian C-4 tiltmeters are orthogonally placed near the base
of each of the ALS geosensors, thus approximating motions of
each gyrocompass IA with base motion measurements. As a part
of an accuracy improvement program, tiltmeters were installed
inside the geosensors across the gimbal axes to better represent
the actual tilts being sensed by the gyrocompasses. Tilt and
tilt rate corrections were applied after the fact during data
reduction. This process can be automated, and real-time cor-
rections applied in the future.

1.3.4 AZIMUTH TRANSFER

Azimuths are transferred from the ALS geosensors to the
desired target by combining the horizontal angle between each
geosensor and the target with the respective ALS azimuth. The
required angles are determined by slewing an autocollimator
mounted on an inductosyn indexing table between each of the mir-
rors once during every measurement position. The inductosyn
slew is commanded by the microprocessor and is triggered when
the microprocessor receives a "servos null" signal from the
ALS.

A predictor scheme is employed to position the inductosyn

so that each time the autocollimator is slewed, it is position-
ed nearly normal to the particular mirror it is sampling. A
servo loop is then activated, allowing the autocollimator to
null on the target by further slewing the inductosyn table.
The final position of the inductosyn table at the target is
combined with the inductosyn table position for each of the ALS
geosensor mirror observations to determine the angle between the
target and the ALS. These angles are then combined with their
respective ALS azimuth estimates to arrive at two redundant es-
timates of each target azimuth. Each new target orientation is
then used as a predictor for the next measurement position, and
the entire cycle is accomplished once again.

1.3.5 DATA COLLECTION AND OPERATIONAL CONTROL

An LSI-11 microprocessor was employed to control opera-
tion of the ALS and inductosyn/autocollimator angle transfer
system. In addition, the LSI-11 acted as an input/output device
for all data handling and operator control commands. Data were
accumulated in the LSI-11 memory and then periodically dumped on
magnetic tape. Analog data were digitized and filtered by the
microprocessor prior to storage. Data reduction was then ac-
complished after the fact in the laboratory.

1.3.6 SYSTEM ACCURACY

Azimuth accuracy of the AAMS is dependent upon both the
system's repeatability (or relative accuracy) and bias (or ab-
solute accuracy). Laboratory and field data have been statis-
tically analyzed to determine the repeatability of the AAMS.
The standard deviation of a single AAMS determination (4 se-
quences) is approximately 2.1 arc seconds. The standard error
of the mean is 0.6 arc seconds. These statistics were deter-
mined by combining the standard deviations from multiple sets

- 9 -

of 4 hours of tilt- and tilt-rate corrected data. Four hours
of data (12 points) was chosen to get a maximum number of points
while minimizing the likelihood of motion of the observed target.

To arrive at the absolute accuracy of the AAMS, one must
simply apply a bias to each determination. The bias would be
determined by calibrating the AAMS against an azimuth standard.
The true uncertainty of a single AAMS observation would then
equal the root sum square of relative AAMS variance and the
variance of the azimuth standard. An approximation of the bias
of the two ALSs was obtained by making repeated azimuth determin-
ations in the ALS certification room at the Aerospace Guidance
and Metrology Center (AGMC), Newark AFS, Ohio, in January and
February of 1976.

A more precise evaluation of the absolute accuracy of
the AAMS was conducted in the early fall of 1978. The AAMS
was referenced to two optical cubes located in the ALS verifi-
cation facility at F.E. Warren AFB, Wyoming. The AAMS data were
compared with repeated astronomic azimuth observations and ALS
certification data available from the Defense Mapping Agency
Geodetic Survey Squadron. In addition, tilt was measured on the
monolith which supports the azimuth reference in order to
further characterize the azimuth motions of the reference cubes
during the AAMS calibration.

1.4 APPLICATIONS

The AAMS is ideally suited for high-accuracy indoor azi-
muth measurements where access to celestial references is re-
stricted. Because of its portability and size, it can be
utilized in confined environments or it can be adapted to
large laboratories where multiple azimuth references are de-
sired.

1.4.1 MINUTEMAN III MISSILE ALIGNMENT EXPERIMENT

One contractual application of the AAMS was to verify the performance of a Minuteman III missile guidance system in an engineering silo. For this experiment, the AAMS was operated inside the missile silo, and was used to track relative motions of the missile by observing a mirror attached to the missile frame. The roll gimbal notch attached to the missile frame is the primary azimuth reference for Minuteman III missiles. Thus, by monitoring the relative motions of the missile frame mirror with the AAMS, the motion characteristics of the missile azimuth reference were defined. Motion scenarios observed during the experiment included missile nozzle tests, missile inertial measurement unit calibrations, two distant earthquakes and motions due to thermal variations. These data were then compared with azimuth alignment data from the onboard gyrocompass assembly (GCA). The GCA data reflected how the missile guidance set interpreted the motions of the *azimuth* reference. The comparison of the two sets of data therefore provided a means for evaluation of the effectiveness of the missile in maintaining its azimuth orientation under various motion scenarios.

AAMS data, uncorrected for tilt and tilt rate errors was collected during a weekend interval when the silo was unoccupied. Corrections for the effects of tilt and tilt rate which were applied to the raw ALS azimuth estimates were then made. These corrections were determined by computing the theoretical effects of the measured tilts on the ALS gyrocompasses at 41°N latitude. For this application, a tilt error of 1 arc second caused an 0.87 arc second azimuth error. A tilt rate of only 0.2 arc seconds per hour induced a 1.0 arc second gyrocompassing error. One can determine that most of the apparent diurnal motion observed in the raw ALS azimuth estimates resulted from tilt rate errors caused by solar heating of the ground surrounding the silo. The tilt correction, however,

exhibits a long period trend of nearly 4 arc seconds. This correction resulted from a gradual tilting of the silo collimator bench (which served as a support for the AAMS) due to a rise in the ambient silo air temperature.

Application of the combined tilt and tilt rate corrections to the raw azimuth estimates results in the actual missile mirror azimuth time history. Diurnal effects which became apparent were removed by applying corrections. The validity of applying theoretical tilt and tilt rate corrections to raw ALS azimuth estimates was verified experimentally. A single ALS was placed on a tilt table at Weston Observatory, Weston, Massachusetts. After the ALS had reached thermal stability (24 hours continuous operation), the table was tilted 6.18 arc seconds (600 table counts). The mean values of the ALS azimuths for a period of eight hours before and eight hours after tilting the table were computed. The difference between the mean before and the mean after agreed within 1.8% with the theoretical azimuth change caused by the calibrated tilt. A similar experiment was conducted to determine the effects of tilt rate. The table was operated through its range in both directions at a known rate. Once again the differences in the means of the azimuths for the periods when the table was being tilted were compared with the theoretical azimuth changes. The agreement was within 3.4% and 0.7% respectively for the two directions.

i.4.2. CENTRAL INERTIAL GUIDANCE TEST FACILITY

Another application of the AAMS was to determine the azimuthal motion characteristics of two azimuth references at the Air Force's Central Inertial Guidance Test Facility (CIGTF), Holloman AFB, New Mexico. For this requirement, the azimuths of two reference devices - a porro prism mounted on a granite monolith and a mirror mounted on a precision Goerz tilt table were measured. Previously, the means for determining the

azimuths of these references was through a combination of (1) celestial observations from the roof of the building using a Kern DKM-3 theodolite, (2) double autocollimation through a sight tube to a second DKM-3 theodolite, and (3) a third pointing of the theodolite to the porro prism. Transfer of the azimuth to the Goerz table required an additional relocation of the theodolite and a series of direction observations between the porro and the Goerz mirror.

By employing the AAMS with autocollimator observations of both the porro and the Goerz mirror during each sequence, the azimuthal motions of both references could be characterized and compared. Azimuthal motions with diurnal periods are of special interest at this facility because of the termperature extremes between day and night. Tilts of several arc seconds have been observed on the granite monolith where the porro prism is mounted. Thus,it is reasonable to suspect that azimuth changes of this magnitude may also occur.

1.5 GEOSENSOR

In addition to the tiltmeter array used to monitor bending of the AAMS geosensor mounting plate, new tiltmeter units were installed directly on the geosensor gimbal assemblies. The design chosen for the AAMS application was a straight line level device. This unique device operates on the principle of straight line translation of a mass with a slight rotation about the direction of travel. The path of the sensing element, being essentially in a straight line, eliminates problems of non-linearity encountered using pendulum-priciple devices. Other advantages include durability, high temperature operation and low drift characteristics. The custom tilt sensing elements designed for the AAMS are capable of detecting a tilt angle of one nanoradian with a long term drift of less than one hundred nanoradians per month. Mounted on the geosensor gimbal,

the effects of microseisms and temperature variations limit the minimum discernable tilt. The software flexibility of the computerized AAMS will be used to optimize the sampling of the tilt data.

1.6   ELECTRONICS

Studies indicated that substantial internal electrical noise was present on the low voltage supply lines feeding the critical measurement circuits. Unfortunately, the nature of the d.c. supply contributed significant switching transients at the frequency of the converter, which in turn was synchronized to the system clock. The result was the presence of noise pulses on nearly every signal path in the ALS electronics. Experiments involving the application of external d.c. to certain control circuits eliminated much of this noise. Tests showed a reduction in the variability of the measured azimuth readout when external linear power supplies were utilized. In order to insure the quietest operation of the electronic networks, precision linear power packs were devised to provide all d.c. power for the ALS. These power packs were integrated with the power control circuits for normal operation.

1.7   OPTICAL TRANSFER

A considerable improvement in pointing accuracy of the electronic autocollimator was obtained by introducing low velocity air along the line of sight. Use of sight tubes over distances greater than 20 feet was studied and it became apparent that this was a very complex problem. Lightweight, thin-wall tubing was far too flexible, and thick-wall tubing was far too heavy. Additional problems arose in determining methods of tube support and the effects of internal wall reflection. The method of introducing forced air into the sight tubes and the

optimum flow velocity were also studied. Preliminary examinations of these problems indicated that it was counter productive to continue the investigation of long-length sight tubes.

1.7.1 OPTICAL TABLE

For previous field operations, the AAMS was supported by a 1" X 3' X 5' steel plate which was found to be very sensitive to thermal gradients between its top and bottom surfaces. Distortions of several arc seconds of tilt resulted from temperature gradients of as little as $0.1^{o}C$. As a result, the two geosensors, Goerz Inductosyn, Porro prism and surface tiltmeters were subsequently mounted on a special optically flat table. This table was 1m X 3/4m X 100mm and it was made of aluminum honeycomb construction with a stainless steel top and bottom skin. Locating lugs insure that the same relative alignment could be achieved each time the equipment was set up at a field site. The honeycomb construction gave a stable mounting base with the strength of a steel plate, but at much reduced weight and thermal sensitivity.

1.8 GYRO OPTIMIZATION

Two conditions affect the performance of the gyrocompass: transient effects and gyro drift. Transient effects result from wide angle displacement of the gyro signal generator during the normal slew cycle. First, the rebalance torque was found to be insufficient to hold the signal generator at null in the presence of a high slew rate. Second, a thermal imbalance resulted from a redistribution of the floatation fluid around the float heaters following float rotation. These effects decay with time. Gyro drift can be both random and systematic. Random drift results in noise in the rebalance torque signal; this error will be averaged rather than accumulated.

- 15 -

Systematic drift has a bias term which accumulates with time. These error terms have been found in similar gyros. However, the specific characteristics for these gyro drifts for the two ALS gyros now in use in the system are unknown. The AAMS electronics were designed to allow a wide variation of gyro settling and sampling times. The optimum values for minimum variation in the azimuth data were obtained.

1.9 CONCLUSION - SYSTEM AUTOMATION

The ALS control indicator contains the measurement and sequencing circuits, and all functions are synchronously locked to the master clock. Once started, the gyrocompass sequence proceeds automatically as dictated by the timing circuits. The two ALS systems were synchronized by a fairly complex electronics package which required frequent maintenance. The assimilation of logic signals from the geosensor and related sequencing circuits is ideally suited for local microprocessor control. If upgrade of the system is considered at some time in the future, command and control of the geosensor and gyro torquer loop should be assigned to dedicated LSI-11/2 microprocessor modules. This would facilitate software control of system functions with flexibility for interactive operation for evaluation and diagnostic procedures. Synchronization of the dual geosensors would be greatly simplified and the reliability of operation improved. Basic support circuits (gyro spin motor supply, gimbal servo loops, and temperature control) should be retained in the original control indicator units. The LSI-11/2 microcomputer, with memory modules for storage of the four position gyrocompass sequence program, would then be superimposed on the existing circuits. The microcomputer interface with the geosensors and control circuits could be achieved through parallel line interface boards. A local control console would allow for manual operation for calibration and troubleshooting.

The crucial gyro torque-loop signal development could be
modified to employ recently developed VFC (voltage to frequency
converter) integrated circuitry. The pulse rate proportional to
torque current thus generated would go directly into the micro-
computer random access memory for azimuth determination. As a
result, the central control function would tie the two channels
of the AAMS together functionally. It would contain the bulk of
the support electronics, including linear d.c. powerpacks, In-
ductosyn table drive electronics, autocollimator electronics,
control indicators, video data display and switches for manual
operation. During normal operation a remote data acquisition
system could handle functional control, local plotting and an-
alysis of small segments of data as well as data storage. The
remote facility would incorporate a stand-alone microcomputer,
magnetic tape data storage and a printer/plotter.

REFERENCES

1. Atwill, W. D., <u>Research on An Automated Inertial Azimuth Measuring System</u>, Boston College Scientific Report No. 1, November 1978, AFGL - TR-78-0285.

2. <u>Proceedings, 1st International Symposium on Inertial Technology for Surveying and Geodesy</u>, Ottawa, Canada, October 1977.

3. Schnelzer, G.A.,Cabaniss, G.H.,and Anthony, D,,"Azimuth Alignment Experiment", <u>Proceedings, AIAA Guidance and Control Conference</u>, San Diego, California, August 1976, AIAA No. 76-1963.

4. Shearer, J.A. and Anthony,D:, <u>Long-Period Azimuthal Motion Effects on Minuteman Upgrade Missiles</u> (SECRET), Air Force Geophysics Laboratory, Hanscom AFB, MA.,1978.

5. Schnelzer, G.A.,Anthony, D. and Cabaniss, G.H,,<u>Long-Period Motion Effects on Service Test Model Azimuth Laying Set (STM-ALS) Gyrocompassing. Minuteman Silo Motion Study</u>, Hill AFB, UT, 1974, Vol 1, AFCRL-TR-75-0402

6. <u>Long-term G1-T1-B Test Report</u>, Northrop Corporation Electronics Division, Norwood, MA, Report No. PPD-71-E-10315, July 1971.

2. INTRODUCTION - CHARACTERIZATION OF ACOUSTIC POWER SPECTRA

Data acquired at Vandenberg AFB were used to estimate the acoustic impedance of various locations at Space Launch Complex (SLC) 6 in support of the Space Transportation System (STS). Predicted STS launch pressures were extrapolated from Titan III - D launches using scaling factors provided by the Aerospace Corporation. Launch pressure data were also analyzed to determine the nature of the pressure field. Coherence between measurements at various distances from the launch was calculated to predict seismic response at various distances from the launch pad. This information was forwarded to Aerospace Corporation to assist in their simulation of the STS pressure envelope. The Aerospace Corp. STS pressure data were then used by Boston College to predict ground motion in the vicinity of the Payload Preparation Room (PPR) and Launch Control Center (LCC). Predicted vertical and radial components of ground acceleration were provided to Parsons Corp. in conformance with SAMSO specifications.

Pressure and seismic data analysis of the Titan III - D launches continued with emphasis on the coherency of the launch pressure field. The seismic response is sensitive to the phase velocity of the pressure field. In turn, phase velocity is a function of the height of the rocket. Post-launch measurements were analyzed, and standardized to a reference seismometer. Plots of this data and corresponding spectra were provided to AFGL for presentation at Vandenberg AFB. Data analysis support was also provided to AFGL in conjunction with their MX studies being carried out in the southwestern United States.

Data analysis activities continued in support of Space Transportation System facility design. Characteristics of Titan III -D induced surface pressure were analyzed by fitting

a theoretical model to the power spectral density of the observed pressure at various intervals during launch. Investigations were continued so as to gain a better understanding of fitting theoretical curves to the Titan launch data. Simulated data were generated by filtering normally distributed noise with the spectral form of the theoretical function. Fits to these data were made in order to develop a goodness of fit criteria.

2.1   CHARACTERIZING PRESSURE SPECTRA

To obtain estimates of the power spectral density at a given time after ignition, 256 samples were read-in beginning at that time. These samples were digitized at 204.8 counts per volt. The power spectra were computed by the periodogram technique employing an FFT algorithm. This periodogram was such that

$$\frac{1}{N} \sum_{i=1}^{N} x_i^2 = \sum_{k=1}^{N} s_k .$$

It was found that the noise caused by the system and ambient pressure fluctuations was white and assumed to be additive above the quantization level. This was estimated by averaging 20 periodograms starting 1 minute before launch and it was found to be: $9.37(10^{-8})$ volts^2 per cell. This noise term was subtracted from the rocket spectra to yield the best estimate of rocket induced surface pressure observed through the system. These spectra were converted to the spectra appearing at the input. To reduce contamination from errors in our estimate of system behavior near the Nyquist frequency, only frequencies less than 40Hz were considered.

From physical considerations and experimental studies it is believed that the power spectral density of the pressure caused by undeflected chemical rocket plumes is of the form:

$$P(w) = \frac{4}{\pi} \frac{P_{max}}{W_0} \left\{ \frac{W}{W_0} + \frac{W_0}{W} \right\}^{-2} \quad \text{or} \quad P(f) = \frac{4}{\pi} \frac{P_0}{f_0} \left\{ \frac{f}{f_0} + \frac{f_0}{f} \right\}^{-2}$$

It was desired to obtain values of P_0 and f_0 which minimized E
(E=error) the sum of the squared differences between the observ-
ed power spectral density and the theoretical as described by
the above equations.

The optimum f_{Opt} and P_{Opt} were values used to generate
plots showing power spectral density based on observed values
and theoretical values vs normalized frequency, f/f_0.
Table 1 shows f_{Opt} and P_{Opt} for a number of launch time seg-
ments.

In order to compare average observed power with theoreti-
cal power the theoretical power spectral density was integrated
from $-\infty$ to ∞.

$$P_t = \int_{-\infty}^{\infty} P(f)\,df = \frac{4}{\pi} \frac{P_0}{f_0} \int_{-\infty}^{\infty} \left(\frac{f}{f_0} + \frac{f_0}{f}\right)^{-2} df$$

$$= \frac{4}{\pi} P_0 f_0 \int_{-\infty}^{\infty} \frac{f^2}{(f^2 + f_0^2)^2}\, df$$

$$= \frac{4 P_0 f_0}{\pi} \left\{ -\frac{1}{2} \frac{f}{(f^2 + f_0^2)} \Big|_{-\infty}^{\infty} + \frac{1}{2} \int_{-\infty}^{\infty} \frac{1}{(f^2 + f_0^2)}\, df \right\}$$

$$= \frac{2 P_0 f_0}{\pi} \int_{-\infty}^{\infty} \frac{1}{(f^2 + f_0^2)}\, df = \frac{2 P_0 f_0}{\pi} \left(\frac{\pi}{f_0}\right) = 2 P_0$$

The observed power $(\Delta f \sum_{k=1}^{129} P'_k)$ and theoretical power are contain-
ed in Table 1.

2.2   VALIDATION

Although the theoretical curves do not appear to closely
fit the observed spectra, it is known that the periodogram is an
inconsistant unbiased estimator. It was desired to test whether

- 21 -

the observed fluctuations fall within expected limits when the
theoretical power spectral density is assumed true. Oppenheim
and Schafer show the development of an expression for the vari-
ance of the estimated P_k' 's for a white Gaussian process. They
state that the variance (σ^2) of the spectrum is approximately
equal to its magnitude squared.

$$\sigma_k^2 = \frac{1}{M}\sum_{m=1}^{M} (P_k'^{(m)} - \overline{P}_k')^2 = \overline{P}_k'^2$$

or

$$\frac{\sigma_k^2}{P_k'^2} = \frac{1}{M} \sum_{m=1}^{M} \frac{(P_k'^{(m)} - \overline{P}_k')^2}{\overline{P}_k'^2}$$

A figure of merit is defined as $\quad \dfrac{1}{102} \displaystyle\sum_{k=2}^{103} \dfrac{\sigma_k^2}{P_k'^2}$

which with $M=1$ and $\overline{P}_k'$ assumed equal to $P(f_k)$ becomes

$$\frac{1}{102} \sum_{k=2}^{103} \frac{(P_k' - P(f_k))^2}{P^2(f_k)}$$

This quantity, which should be approximately 1, is contained
in Table 1. In addition, as has been demonstrated, $2\,\dfrac{P_k'}{P(f_k)}$

follows a chi-squared distribution with 2 degrees of freedom
for large N.

As an additional test of the validity of the fit this
criteria was used. For each value of $A_k = \dfrac{2P_k'}{P(f_k)}$ its cumulative

relative frequency was computed.

a_x = estimated probability that $A_k \leq x$.

The chi-squared distribution for 2 degrees of freedom is

$$1 - e^{-\frac{\mu}{2}}$$

- 22 -

Therefore $\mu=-2\ell n(1-a)$

and $\mu_x=-2\ell n(1-a_x)$

For a good fit μ_x should be approximately equal to x. x has been plotted vs. μ_x for each segment.

2.3   RESULTS

Results presented in Table 1 were then plotted. Plots were of the observed spectra (points only) and fitted theoretical curves (solid lines). As previously defined, plots A_k vs μ_x were labelled 'observed test statistic' and 'theoretical test statistic' respectively. The vertical axis was scaled to fit the maximum value of A_k although this point cannot be plotted since its corresponding theoretical value is infinitely large. The horizontal axis stopped at 9.25 which is the 99th percentile for the 2 degree of freedom chi-squared distribution. A solid line represented $A_k=\mu_x$. When the observed points were above the line it meant we had larger values than we should have expected. When they were below it meant they were smaller than expected.

2.4   CONCLUSIONS

In order to determine bounds on the figure of merit for acceptable fits, simulated data were used. A random number subroutine was used to produce normally distributed variables. For each group of 256 numbers the FFT was taken and the magnitude multiplied by the square root of P(f) for a set value of P_0 and f_0. The inverse transform was taken and the result multiplied by a decaying exponential which modelled the envelope of the rocket data. Two hundred similarly produced groups of 256 variables were fitted with the theoretical power spectral density curve and statistics of the figures of merit accumulated.

The figure of merit for this simulation was found to have a mean of 1.07 and a standard deviation of .35. The minimum value obtained was .57 and the maximum was 2.98. It was decided to accept the fitted data if its figure of merit fell within these extrema.

The first fit, which began 3.83 seconds after ignition, produced a figure of merit of 214.6. This fit was rejected. It is believed that because this was so early in the launch the plume was not undeflected, and the theoretical curve did not apply. Figures of merit for subsequent fits fell within extrema criterion and these fits were accepted.

It was found that when f_0 was low (equal to 2.8 Hz) the chi-squared test plot, while a straight line, lay above the $A_k = \mu_x$ line, as happened on a number of the fitted segments and the estimated value of f_0 was high (3.2Hz). Evidently our estimates, while acceptable according to the figure of merit criterion, were biased toward the high frequencies.

TABLE I

Time after Ignition (seconds)	f_0 (hz)	P_0 (psi^2)	$E\left(\left(\frac{\text{psi}^2}{\text{hz}}\right)^2\right)$	Observed Power (psi^2)	Theoretical Power (psi^2)	Figure of Merit
3.83	6.798	$8.477(10^{-5})$	$4.022(10^{-10})$	$7.931(10^{-5})$	$1.689(10^{-4})$	214.6
5.39	14.299	$6.741(10^{-4})$	$1.268(10^{-8})$	$3.875(10^{-4})$	$1.348(10^{-3})$	1.005
6.95	12.071	$1.606(10^{-3})$	$5.342(10^{-8})$	$1.007(10^{-3})$	$3.213(10^{-3})$	.620
8.51	11.190	$1.257(10^{-3})$	$6.848(10^{-8})$	$8.264(10^{-4})$	$2.514(10^{-3})$	1.381
10.07	7.548	$6.361(10^{-4})$	$1.648(10^{-8})$	$4.993(10^{-4})$	$1.272(10^{-3})$	1.528
11.63	5.235	$2.845(10^{-4})$	$5.418(10^{-9})$	$2.572(10^{-4})$	$5.690(10^{-4})$	1.813
13.19	6.097	$1.115(10^{-4})$	$7.147(10^{-10})$	$1.035(10^{-4})$	$2.230(10^{-4})$	1.405
14.75	4.390	$4.608(10^{-5})$	$2.198(10^{-10})$	$4.872(10^{-5})$	$9.216(10^{-5})$	2.59
16.31	2.855	$1.860(10^{-5})$	$9.203(10^{-11})$	$2.420(10^{-5})$	$3.719(10^{-5})$	1.032

REFERENCES

1. Hartnett, E.B. and Carleen, E.D., <u>Characterization of Titan III - D Acoustic Pressure Spectra by Least-Squares Fit to Theoretical Model</u>, Boston College Scientific Report No 2, January, 1980, AFGL-TR-80-0004.

2. Powell, A., Theory of Vortex Sound, <u>Journal of the Acoustical Society of America</u>, <u>Vol</u>. 36, No. 1, Jan. 1964.

3. Acoustic Loads Generated by the Propulsion System, <u>NASA SP-8072</u> June 1971.

4. Burington, R.S.,<u>Handbook of Mathematical Tables and Formulas</u>, Fifth Edition, McGraw-Hill Book Company, New York, 1973.

5. Oppenheim, A.V. and Schafer, R.W.,<u>Digital Signal Processing</u>, Prentice-Hall, Englewood Cliffs, N.J., 1975.

6. Hinich, M.J. and Clay, C. S., The Application of the Discrete Fourier Transform in the Estimation of Power Spectra, Coherence, and Bispectra of Geophysical Data, <u>Reviews of Geophysics</u>, Vol. 6, No.3, Aug. 1968.

7. Owen, D.B., <u>Handbook of Statistical Tables</u>, Addison-Wesley Publishing Co., Inc., Reading, Mass. 1962.

3. INTRODUCTION - ATTRIBUTES OF SEISMIC TRANSIENTS EXCITED BY RADIATION SHOTS
AT CASINO

The cooperative Boston College/AFGL study described herein was carried
out in direct support of SAMSO's MX/TGG Advanced Development Bridge II Pro-
gram for radiation hardening the Third Generation Gyro (TGG). As part of this
program, TGG performance tests in a radiation environment were conducted at the
CASINO Facility in Silver Spring, Maryland. CASINO is a Defense Nuclear
Agency (DNA) sponsored facility that can simulate those electrical and mech-
anical effects in components which are produced by the radiation output from
nuclear weapons. For the TGG test, it was required to isolate radiation ef-
fects from seismic side effects generated by the CASINO machine. Evaluation
of these seismic side effects and precautionary measures against them di-
rectly concern the TGG test result. The investigation addressed itself ex-
clusively to the nature of the seismic motions within the CASINO exposure cell
excited by radiation shots.

3.1 DESCRIPTION

The Hall-Sears model 10.1 seismic sensor was used in the study. In a
preliminary study at CASINO we found that this transducer gave a negligible
output for hot shots with the suspension locked. Calibration of these sen-
sors was made both before and after measurements to insure that the sensor
was not altered by repeated exposure to radiation (a sensitivity loss of 16%
was experienced over the test sequence). The nominal response of the measur-
ing system to a velocity of the sensor base along its sensitive axis was cal-
culated. Viewed in terms of "acceleration", the sensor gain decays at a rate
of 6 db/octave above 1 Hz. For the horizontal sensors, the acceleration in-
put is either one of two terms; a translation and an acceleration component
due to tilt. In this study, the acceleration component contribution due to
tilting was found to be negligible.

Using an array of seismic sensors and a stand with a distortion free
plate, rotational and translational motion due to "radiation shots" were sep-
arately estimated. In these calculations, system responses were forced to

be equal by post processing the measurements by the appropriate correcting operators. These correcting operators were determined by measuring the output of "colocated" sensors during shots. Further, for the measurements presented here, the observations were generally band passed to $1 < f < 50$ Hz. Motions at lower frequencies are small but can be included in our ongoing analysis. Motions much above 50 Hz are generally beyond a frequency that can be reliably measured by these transducers. Further, for frequencies much above 50 Hz, the test stand plate will not remain distortion free.

3.2 TRANSIENT MOTION - CASINO PIER

Transient seismic energy levels within the CASINO shielded test room were more pronounced from firings utilizing the water switch. For those firings not employing the water switch, the seismic energy levels were consistently of an order of magnitude lower. In a preliminary study it was found that the motion of the seismic pier from firings of the CASINO machine was almost purely translational. Further, the seismic transients generated by those firings were found to be highly reproducible. Seismic pier motion following a radiation shot was found to decay in exponential like fashion with a time constant of less than 1 second. That is, the amplitude of the seismic disturbance fell to less than 37% of its initial peak value in less than one second following a shot. The maximum accelerations of the seismic pier and their respective decay times are summarized in Table 1.

Table 1

Component	Peak Velocity	Peak Acceleration*	Decay Time
x	1.08 mm/sec	137 mm/sec/sec	.5 sec.
y	.94 mm/sec	130 mm/sec/sec	.9 sec.
z	1.46 mm/sec	342 mm/sec/sec	.4 sec.

* 9806 mm/sec/sec $\approx$ 1g

3.2.1. SPECTRAL ATTRIBUTES - TEST PIER

Seismic pier velocity transients produced by a firing were spectrally analyzed. It was determined that the bulk of the seismic energy over the primary pass band, (5 - 50 Hz) was clustered in bands around 20 and 35 Hz. The seismic pier motion reflects the response of the housing structure. If the building, foundation and source are common between shots, the resulting seismic disturbance is repeatable even in its fine structure. Further, since there is a high degree of symmetry in the seismic aspects of the problem, one can expect a common spectral content as different machines are fired. Only the phase of the disturbance should be altered. The uniformity of the seismic transient should be considered for further study since it is an important underlying assumption to the TGG test rationale.

3.3 TRANSIENT MOTION - NORTHROP TEST STAND

Of immediate concern to TGG testing is the seismic transient impinging on the unit mounted in its holding fixture. One consideration in the design of the test stand was that it should provide stiff coupling between the TGG and the seismic pier to ensure that the stand would not appreciably amplify or increase the time constant of the seismic transient. The aim here was to construct a stand whose eigenfrequencies were well in excess of 50 Hz. The motion level of the stand was held to those of the seismic pier over the primary pass band (<50 Hz). For this element of the problem, the test stand met its design objective; the first serious stand response was found to be well above the highest frequency of concern.

3.3.1. TEMPORAL AND SPECTRAL PROPERTIES - NORTHRUP STAND

In our measurements, the sensors were arrayed and combined to separate rotations from translations under the assumption that the test stand's surface remained strain free over the primary pass band $1 < f < 50$ Hz. For this assumption, rotation is insensitive to the TGG's location on the plate.

The resulting peak angular velocity $\dot{\varnothing}_z$, was found to be 406 $\stackrel{\frown}{\sec}$/sec. The transient is narrow banded with a decay time of approximately 1 second.

3.3.2   SEISMIC ATTRIBUTES OF THE NORTHRUP TEST STAND ARE SUMMARIZED IN THE FOLLOWING TABLE:

Table 2

Component	Shot # 518 Peak Value	Stand Dominant Frequency
$\dot{\mu}_x$	4.27 mm/sec	22, 35 Hz
$\dot{\mu}_y$	3.96 mm/sec	33,35
$\dot{\mu}_z$	1.70 mm/sec	33,22,15
$\ddot{\mu}_x$	678 mm/sec/sec	35,22
$\ddot{\mu}_y$	716 mm/sec/sec	35,33
$\ddot{\mu}_z$	364 mm/sec/sec	37,33
$\dot{\varnothing}_x$	313 $\stackrel{\frown}{\sec}$/sec	35
$\dot{\varnothing}_y$	277 $\stackrel{\frown}{\sec}$/sec	35,22
$\dot{\varnothing}_z$	406 $\stackrel{\frown}{\sec}$/sec	35

3.4   CONCLUSIONS AND RESULTS

Unlike the preliminary study, there appears to be significant differences in stand motion from shot to shot. These apparent differences should be the subject of continuing study. Further, if required, stand motion can be put into a more convenient form; example, the gyro coordinant frame. Low frequency tilting of the stand appears as a random variable. As such, hardware has been provided to include "tilt" as an observation within the TGG testing

effort.

The following results are based on seismic measurements taken at the CASINO Facility caused by firings.

    a.   Principal part of seismic energy over the band 1-50 Hz is concentrated near 20 and 35 Hz

    b.   Transient motions on the seismic pier are almost purely translational

    c.   Test stand surface motion is both translation and rotation

    d.   Test stand rotations are confined to 22 and 35 Hz

    e.   Significant differences appear in stand motion for repeated shots

    f.   Test stand horizontal motion is substantially larger than that of the seismic pier

    g.   Test stand surface horizontal rotation is larger than vertical rotation

    h.   Translational motion on test stand surface is a fu: ction of postion

    i.   Decay time constant for all events < 1 second

    j.   Low frequency tilting appears as a random variable

3.5   HS-10-1 MOTOR CONSTANT CALIBRATION

Motor constant determinations were made for the Geo-Space HS-10-1 seismometers used in the CASINO study prior to and after radiation exposure. Nine sensors were employed and tested. The calibration technique was the mechanical weight-lift electrical equivalent comparison method. Briefly, a small test weight (2 grams) was applied directly to the seismometer mass, and quickly removed. The resulting voltage output transient was measured and retained on a storage oscilloscope. An equivalent step in current was applied to the seismometer via a calibration circuitry. The original mechanical weight-lift

waveform could be duplicated in both amplitude and polarity. Knowledge of the weight removed and the current drop across the seismometer terminals required to duplicate the mechanical weight-lift provides sufficient information for determining the seismometer motor constant via the relation $G = Wg/I$.

The pre-CASINO mean motor constants for the nine seismometers at CASINO was computed as $\overline{X} = 1089$ N/I having a standard deviation of $s_x = 64.56$. Post-CASINO mean clibration was $\overline{x} = 932$ N/I with a standard deviation of $s_x = 56.63$. The observed 16% drop in the Post-CASINO mean was attributed to radiation and/or electro-magnetic pulse effects on the seismometer magnet.

REFERENCES

1. Crowley, F., Ossing, H., and Hartnett, E., March,1978, The Attributes of Seismic Transients Excited by Radiation Shots at CASINO, AFGL Technical Memorandum No. 10.

2. Crowley, F.(1978) Motions of Seismic Block Caused by Hot Shots at the CASINO Facility, Naval Surface Weapons Center, White Oak Laboratory, Silver Spring, Md., Memorandum dated 12 December 1977.

3. Crowley, F., and Ossing, H., (1970) An Analysis of the Vibration Environment with Appliecation to Single-Degree-of-Freedom Gyroscope Performance Tests, AIAA 70-951, AFCRL-70-0476.

4. Crowley, F., et al (1970) An Analysis of the Vibration Environment at Northrop's Norwood Mass. Test Facility with Application to Gyro Testing, AFCRL-70-355.

4. INTRODUCTION - STAND ALONE DATA ACQUISITION SYSTEM (SADAS)

The Stand-Alone Data Aquisition Systems (SADAS) are transportable micro-
computer based systems developed as part of the Geokinetic Data Acquisition System.
The SADAS were designed to acquire data at rates of up to 100 samples per
second from both analog and digital geophysical instruments. Up to 16 chan-
nels of analog data and 150 bits of digital data can be recorded with a
throughput rate in excess of 1600 samples per second. Sampling parameters
can be altered and verified by the operator through the system command con-
sole, which can also provide real-time display of the data being acquired.
Data are stored on floppy disks and industry compatable magnetic tape. The
central parts of the SADAS systems are the LSI-11 microprocessor and its
associated I/O bus. This bus connects the microprocessor with all peripher-
al devices in the system. The devices attached to the bus can be broken
down into four classifications: the LSI-11 microcomputer system, data ac-
quisition devices, storage devices, and devices associated with operator com-
mand and control (A brief description of these functions follows).

(a). LSI-11: A 16 bit microcomputer component consisting of a micro-
processor, dynamic memory, serial interface units, parallel
interface units, system bootstrap module, system backplane
and power supplies.

(b). DATA ACQUISITION DEVICES: Two peripherals dedicated to tak-
ing analog and digital data, one of which also provides sam-
pling frequencies. In addition to these devices, the proto-
type system used with the AAMS has two devices devoted to
acquiring digital data.

(c). STORAGE DEVICES: There are two types of mass storage devices; a
magnetic tape recorder for data acquisition storage and a dual
drive floppy disk functioning as a program storage device.

(d). COMMAND AND CONTROL: Typically, two terminals are utilized for

operator command and control. Through these terminals the operator can
inspect and modify sampling parameters, and check the overall status
of the daa acquisition program. Real-time displays of analog data
are also provided by these terminals.

Improvement of the SADAS developed under previous contracts was con-
tinued. The Kennedy recorder interface was modified to correctly transmit
the end of signal flag during read requests. An intermittant writing problem
in the Kennedy recorder was found to be caused by a hair-like break in the
etch of a printed circuit board that controls part of the unit's write func-
tion. A complete SADAS was sent to AFGL for modification before shipment and
deployment near Miser's Bluff, Arizona. AFGL generated test tapes for the
Kennedy recorder were verified at Weston. Previous recording difficulties
were corrected by inserting differential line drivers and receivers in the
Kennedy / LSI-11 interface.

4.1   MISERS BLUFF/STEPTOE VALLEY STUDIES

4.1.1. LOCALLY INDUCED AMBIENT MOTION

Preliminary data acquired in the June 1978 test shot in support of the
MX Program indicated that the Miser's Bluff area had more seismic noise than
expected. In order to study this noise, amplifier gains were reduced and
new software was developed to record segments of data spaced over long peri-
ods of time without operator intervention. Also, the data acquisition soft-
ware was modified to compute running sums of input data. Several tapes of
ambient noise were obtained. Subsequent analysis of this noise showed that
the high motion levels were caused by several local sources such as passing
freight trains and trucks.

4.1.2.   APPROACH

The stand alone system was installed at the South Steptoe Valley site
in April 1980 and calibration data were acquired. Background noise was sam-

pled at regular intervals and stored on floppy diskettes. "Hammer Blow" tests were conducted near the instrumentation array. Data were collected using the hammer-mounted accelerometer as the input for the computer sample program. Data collected in this experiment were used to compute the Green's function for this area.

Seismic data collected at a site geologically typical of potential MX siting locations were also analyzed. Ground response from "Hammer Blow" tests held in conjunction with Boeing's test runs was used to generate an operator which computes force applied to the ground. This operator was applied to several vehicle runs.

4.1.3. DATA PROCESSING

Cal data were processed by two different software routines for determining seismometer poles and damping factors. The first routine (CAL) is a binary search routine that finds a pole with damping and gain to an accuracy of .5%. This program can be executed to process data from a single seismometer or can be called by a batch file to process data from up to 16 seismometers. Execution time is approximately 35 minutes per seismometer. The second routine (CALYEC) performs the same function as CAL but uses a much slower and more straightforward search technique. Specifically, the program evaluates every pole-damping pair in a user-specified range to a specified accuracy. Results of processing the cal data with this program were used as a check of the CAL programs's results. The findings indicate that the quicker CAL program gives identical results and is therefore more suitable for field applications.

Response of the data acquisition system used in support of the MX program at Parker, Arizona was examined and found to be acceptably close to the theoretical response. A measurement of system noise was obtained and used in the data analysis processes. Further analysis of the Parker data showed that during events, such as trucks or trains passing by, the observed phase velocity across the array of instruments could be used to compute horizontal refraction for the area.

4.1.4 CONCLUSION

In conclusion, to a first approximation, base level particle velocity in Steptoe Valley, Nevada can be represented as the convolution of an orientation sensitive valley response function with a stationary, independent, zero mean, three dimensional orthonormal, gaussian process.

Over the band $3 \leq f \leq 30$ Hz, the RMS value of the ground particle velocity for intervals free of conspicuous events is approximately equal to 10 m μ/sec times the square root of the measurement bandwidth. The motion level in Steptoe Valley is significantly larger than that commonly ascribed to teleseismic detection stations in the basin and range province.

REFERENCES

1. Ossing, H.A. and Gray, R.A. (1978) A Survey of the Ambient Motion Environment in the Southwestern United States (1978) AFGL-TR-78-0052.

2. Crowley, F.A., Ossing, H.A., and Hartnett, E.B., Temporal Attributes of Seismic Base Noise in Steptoe Valley, Nevada (1980) AFGL-TM-80-40.

3. Syverson, C.R., Blaney, J.I., Hartnett, E.B., and Molineux, C.E., Geokinetic Environment Studies, (1977) AFGL-TR-78-0124.

4.2. HILL ENGINEERING TEST FACILITY DATA ANALYSIS

4.2.1. MISSILE GUIDANCE SET

This investigation utilized an inert LGM - 30G missile mounted on a CI-10774 Missile Suspension System (MSS) at the Hill Engineering Test Facility, Hill AFB, Utah. The Launch Facility (LF) is a full scale simulation of a Wing V complex. For our purposes, the system studied differed from an operational system in two respects. One, the total mass and mass distribution differed slightly from a Wing V system in that no compensating mass was installed to simulate the reentry vehicle. Two, the LF was the center of a number of other activities atypical of an operational silo; much of the time the LF personnel access hatch was open.

The omission of a reentry vehicle leads to small predictable shifts in the frequencies of the main contributing modes of missile roll. For roll at least, the small difference in the response of the MSS leads only to small differences in missile roll attributes. A more serious concern is that seemingly minor differences in launch tube airflow might lead to substantial differences in missile roll levels. Minor changes in the location of the launch tube heater duct or the amount of airflow can produce a substantial change in the roll torque applied to the missile.

For the weapon system under study the Missile Guidance Set (MGS) consisted in part of a stable platform that was torqued to hold its alignment to the missile roll gimbal while in its normal, prelaunch, ready state. The long term orientation of the platform was then estimated by gyrocompassing. Azimuth error, the difference between the platform's true orientation and the gyrocompass estimate, is insensitive to missile roll for periods greater than something like a day. For these periods, Inertial Performance Data (IPD) tracks the orientation of the missile/platform. This was not at all true for missile roll in the seismic spectrum. The lowest frequency of the seismic spectrum was approximately one cycle per hour. For a missile in roll at seismic frequencies, gyrocompass estimates of platform orientation underestimated the platform's true motion by more than an order of magnitude. Operational IPD was opaque to missile roll induced azimuth error in the seismic

spectrum. This study concentrated on only a portion of the seismic spectrum, one cycle per second to one cycle per minute. For frequencies well below the fundamental of the guidance platform's limit cycle, the roll control loop tends to track missile roll. At frequencies above the platform limit cycle, missile roll more noticeably affects the character of the control loop.

For our present purposes we define a benign, seismic environment to be a state of ground unrest incapable of causing a seismic event detection by a Wing V missile operating in strategic alert. For missiles in Wing V, the seismic environment remains benign if the angle between the missile pitch or yaw gimbal axes and the stable platform accrued over 1.44 sec is less than two gimbal counts. Two gimbal counts can occur once the accrued angle lies in the range of 70 to 140 $\overset{\frown}{sec}$. An angle as large as two gimbal counts in 1.44 sec must be almost exclusively due to missile tilt, once the platform enters steady state leveling – its usual state – for the maximum slew rate of the platform's control loop is 1.075 $\overset{\frown}{sec}$/sec.

4.2.2. APPROACH

The Seismic Activity Monitor (SAM) used in this study is a self-contained automatic system. The most recent data are held in a temporary memory which is continuously updated. Whenever activity exceeds a preset level, or at the operator's command, SAM is activated to record a selectable quantity of data into permanent storage on magnetic tape. Data and time information accurate to the nearest second are included in the data stream. While specifically designed to take data from seismometers, the SAM is actually a general purpose data acquisition system that can be employed for a broad range of applications by providing amplifiers and sensors required for the intended application.

The system accepts analog data for up to 16 channels, but can be short cycled to any number less than 16. The temporary memory consists of 512 six-bit bytes. Two bits in each byte are used for identification code. The 12 bits from each A/D conversion are written as three 4-bit bytes in binary format beginning with the least significant bit.

Amplifiers condition the sensor signals to produce the desired form

for ground motion. The event detector monitors these signals. Whenever one or more outputs exceed a predetermined level, an event pulse is generated. This pulse increments an event counter and triggers a transient mode converter. The transient mode converter then controls the recording into permanent storage for a selected number of data records, beginning with the record in temporary storage prior to the event.

A method was developed for simulating missile roll for a Wing V system operating in a benign, event-free seismic environment. Seismic motion into a Wing V Missile Suspension System (MSS) is translational in that the three silo suspension brackets execute a nearly common motion over the primary passband, 1 cpm to 1 Hz, for a source free area. We therefore treat ground motion into a Wing V MSS as the free field acceleration of a point. Ground motion about a stable point for an event-free seismic environment is simulated by a gaussian, three dimensional, vector process in which orthogonal accelerations $\ddot{\mu}_i$ i= 1,2,3 have definable properties. The power spectra of the component accelerations are defined from the Fourier transform of the correlation of second order, covariance. The ground accelerations generated in this simulation conform to spectral estimates for North American, rural, midcontinental sites. The spectral level is forced to agree with third quartile observations; that is, our simulation spectra should be only exceeded 25 percent of the time for silos within Wing V. The zero order spectral moment for the simulated seismic environment can be determined. Over the band 0 to 5 Hz the RMS acceleration is 0.48 μ gs. The peak ground displacement near storm microseismic frequency is less than 1 micron.

This study yields the main attributes for an event-free seismic environment located in a midcontinental, rural area for moderately noisy times. Motion at such sites and times is the result of a large number of weak seismic disturbances coming from distant, independent, seismic sources well distributed in azimuth about the LF. It is worth noting that the spectra developed here differ from what might be found at any particular Wing V LF in that the effects of local layering and local sources are suppressed. Local ground layering tends to produce a number of site peculiar spectral maxima and minima. For times or for sites where only a few sources dominate, the component accelerations become intercorrelated.

4.2.3. SUSPENSION RESPONSE

For low motion levels and seismic frequencies, we treat the missile
and missile cage as a pair of rigid inertial elements. The missile is coupled
to the missile cage through a system of purely linear, time invariant, spring
and viscous elements. In like manner, the missile cage connects to the silo
solely through linear elements to give a MSS having 12 degrees of freedom.
The eigenvalues and eigenfrequencies of the system are computed from an umdamp-
ed homogeneous equation. The equation of motion can be forced into a more use-
ful, uncoupled form through a weighted modal matrix formed from the columns
of the eigenvectors. An equation was developed utilizing twelve uncoupled
equations in the 12 principal models of the system. In a series of "small
motion" tests, the Wing V MSS was identified as responding to ground accel-
erations in the manner summarized in Fig. 1.

4.2.4. SIMULATED MISSILE ROLL

The Wing V motion model was further refined by inputting ground ac-
celerations expected at a rural, hard rock site into a MSS having the eigen-
frequencies, damping and modal terms given for a Wing V system operating in
a distant attack configuration. A figure was derived showing missile motion
simulation for an event-free, rural midcontinental seismic environment. This
figure showed resultant missile motion in yaw, pitch, and roll due to the sim-
ulated ground motion when the suspension acts at seismic levels in the same
manner found for "small motion" testing. It is worth noting that the seismic
levels in this simulation were substantially smaller than the motion levels
used to define the values in Fig. 1. Further, the response of the missile
in roll, as given in Table 1, was sensitive to an arbitrary mass imbalance as-
sumed for the MSS to produce roll torques. This figure also indicates that
missile motion is a switched-on process that decays to a stationary-gaussian
process for times in excess of the process's correlation time. The correlation
time for the missile in roll is largely controlled by the 80 sec delay time of
the low order modes. For times in excess of a few minutes, this nonstation-
arity decays to a negligible level. The roll process then is stationary-

gaussian, for the MSS is represented by a linear, time invariant operator, and any such operation on a gaussian process in turn gives rise solely to a gaussian process. Being zero mean, stationary and gaussian, the process can be described through its correlation of second order or equivalently the Fourier transform of its covariance, power spectrum.

The roll power spectrum for missile roll rate excited in this simulation was dominated by contributions centered at 0.191, 0.293 and 0.422 Hz. The first two modes, centered at 0.191 Hz, were by far the main contributors to missile roll. This in part was due to the fact that the peak in the ground acceleration spectra closely matched the eigenfrequency of the two lowest order modes. The third and fourth modes at 0.293 Hz contributed about the same amount as the 5th mode. Modal contributions above the 5th mode were found to be quite small. The RMS value for roll over the band 1 cpm to 1 Hz is 0.01 sec RMS. For this simulation, the missile appeared quite stable.

4.2.5. A BENIGN MOTION ENVIRONMENT

Our simulation for a rural, midcontinental, event-free seismic environment is also benign in the sense we have defined it; only rarely will missile yaw or pitch approach the Wing V seismic event detection threshold, > 70 sec. This can be argued as follow: The expected peak maximum for a stationary gaussian process for a specified time can be related to the spectral moments of the process. A graph was made which provided an estimate for maximum pitch amplitude of the missile over time having the spectral moments of the pitch spectrum. For an individual silo, we found the expected maximum annual pitch amplitude was less than 1.7 sec. Missile yaw, in turn was on the average smaller than pitch. The seismic environment was benign; there was only a minuscule chance for missile pitch or yaw to exceed the Wing V seismic threshold in this simulation. A seismic environment of 20 μgs over the band 1 cpm to 1 Hz is required to regularly exceed the Wing V seismic threshold. A seismic background level as large as this is about two orders of magnitude greater than what is typical for a remote, midcontinental site. Ground levels within an order of magnitude of 20 μgs might occur at coastal sites, for example, Vandenberg AFB, but even here microseisms as large as 10 microns are quite extreme.

- 43 -

4.2.6. MISSILE ROLL MEASUREMENTS

Missile roll measurements reported were based on seismometer measurements. Individual seismic transducers respond to a force directed along the sensor's sensitive axis. An "acceleration" input to the seismometer was obtained by normalizing the response to a unit mass. For small input levels, the sensed "acceleration input is:

$$G/M \ i \ (t) + g\psi(t) + \ddot{u}(t)$$

where

G	=	motor constant
M	=	mass
g	=	acceleration of gravity
$\psi(t)$	=	tilt
$i(t)$	=	external current
$\ddot{u}(t)$	=	ground acceleration

As is well known, the individual "acceleration" terms are unobservable at the output of a single sensor. Response can be determined with a seismometer installed on the missile by inserting known currents, $i(t)$, into the sensors with a premeasured G/M. For our measurements, the output of the individual sensors were amplified and shaped to give a response that was "flat to acceleration" from 1 cpm to 1 Hz. Missile motion measurements were taken by seismometers on platforms affixed to the missile at the level of the MGS and at the frustum near the top of the first stage. When taken in combination, the sensors can isolate missile torsion and roll from other missile motions and deformations. Generally, the output of the combined sensors was post integrated to give an overall response flat to roll rate, $\dot{\phi}(t)$, from 1 cpm to 1 Hz. A sample output of individual "acceleration" and $\dot{\phi}$ measurements was graphed which showed seismometer pairs located at the MGS and atop the first stage. Roll observations were depicted as being in phase and equal over our passband. For these observations, the missile behaved as a rigid body as only torsion free missiles are devoid of a roll gradient.

Under these assumptions, we isolated the system noise spectrum by the appropriate Wiener operator. A figure estimating system noise formed by differencing auto-and-cross spectral estimates indicated that both the form and level of the measurement system noise spectrum were reasonable for the components used. By taking redundant measurements, we found that we could extend missile roll estimates into our system noise at low frequencies by about an octave. Missile roll attributes at frequencies less than 1 cpm were the subject of other studies based on autocollimator and gyrocompass measurements.

4.2.7 OBSERVATIONS

The distribution in roll observed over 166 min for the HETF - 1 missile operating in a benign, event-free seismic environment is shown in Fig 2. For these observations, the LF was unoccupied with the personnel access hatch open. Figure 2 is arranged to give a straight line fit for gaussian variates. The plotted distribution is reasonably linear; missile roll is accepted to be gaussian with a mean, m = 0 and a standard deviation, $\sigma \approx 0.48$ sec. The observed distribution was found to be insensitive to the time of measurement over the 60 day observation period. To this extent the process is considered stationary.

A stationary, gaussian process, $N(0, \sigma)$ can be described in terms of its second order statistics. Again we choose to present the second order statistics of roll in terms of spectral estimates. Fig. 3, a spectral estimate in roll rate, shows the MSS to be dominated by a single eigenfrequency centered near 0.43 Hz. The roll spectrum given here is computed from the cross spectra of redundant roll measurements taken at the level of the MGS and atop the first stage. The spectrum is quite stable, having 50 degrees of freedom.

The spectral width of our estimate reflects the limiting resolution of our analysis. The damping of the MSS or equivalently the width of the true spectral peak need not be correctly estimated. The spectral peak found here compares quite well to the 5th mode response used in our simulation. As previously noted, we did not mass compensate the missile with an element equivalent to the reentry vehicle. A corresponding small upward shift in the

5th mode eigenfrequency is to be expected.

The roll spectra generated here differ substantially from those obtained by simulation. The two major disparities are that modes 1 and 2 are observed to be only minor contributors. Further, they have shifted to about 1 Hz. Mode 5 is now the major contributor and its level is greatly enhanced over what was obtained from simulation, as compared to modes 3 and 4. The observed value in roll here is 25 times greater than that obtained from simulation over the band of interest.

For a linear suspension system driven primarily by seismics, we can expect a high coherency between missile roll and the horizontal exterior ground motion. This is not the case here. Missile roll motion and the horizontal ground motion are largely incoherent at the roll frequency. The coefficient of coherence as computed from spectral estimates is:

$$\gamma_{\ddot{\mu}_H \theta}(f) = \left[\frac{P_{\ddot{\mu}_H \theta}(f) \cdot P_{\ddot{\mu}_H \theta}(f)}{P_{\ddot{\mu}_H \ddot{\mu}_H}(f) \cdot P_{\theta\theta}(f)} \right]^{1/2}$$

where

$\ddot{\mu}$ = horizontal acceleration (ground)

θ = missile roll

f = frequency

Like subscripts infer auto spectra and unlike subscripts infer cross spectra. The $\gamma_{\mu_H \theta}(f)$ estimates are quite stable near the roll frequency (50 degrees of freedom). Ground motion is not the cause of missile roll if the MSS is behaving as a linear system at seismic levels. To further clarify the point that the observed roll in not due to seismics, the launch tube airflow system was shut down and the decay in missile roll was noted. The measured decay in the missile roll amplitude with time followed the shut down of the launch tube heater airflow system. The missile roll decayed in the manner of a lightly damped, constant coefficient, linear system with a decay time of 500 sec. The decay time measured was substantially longer than the 50 sec decay time found for this mode at higher level motions. In this test

the airduct was detached from the MSS; missile roll significantly increased when the heater airflow was initially interrupted.

4.2.8 GUIDANCE PLATFORM ROLL AND AZIMUTH ERRORS

Guidance platform roll measurements were taken by a Kollmorgan auto-collimator affixed to the silo. The autocollimator data returned a 1.075 sec/sec platform slew rate for a stationary missile. Platform measurements were taken during an event-free seismic period with the LF sealed and unoccupied. The missile roll mean amplitude measured over the test period is 0.55 sec.

The expected RMS value for platform roll for a stationary missile is slightly more than 1 sec. The apparent effect of missile motion is a modest diminution in the amplitude of the platform's limit cycle. Our results are in harmony with laboratory test data taken at a seismic simulation facility. It is worth noting that the effect of missile motion in a field situation is much the same as that produced in a laboratory setting that employed sinusoidal inputs to simulate missile roll.

For Wing V, the primary mechanization technique is a promising scheme in reducing azimuth limit cycle error under the condition of a benign, event-free seismic environment. For Wing VI, missile roll levels are expected to be too large to make a similar azimuth error reduction by the primary mech-anization technique.

4.2.9. SUMMARY

The launch tube air handling system at HETF-1 is a full scale replica of the air systems used in Wing V. Our results are only directly applicable to a Wing V system with the airduct detached from the MSS, but all else being equal, systems using larger capacity units can expect a larger mean airflow in the launch tube. Torque levels to the missile might relate to airflow as the square of the mean air velocity. For example, airflow within Wing VI is ap-proximately twice that of Wing V. A fourfold increase in roll torque and roll level at Wing VI appears reasonable.

- 47 -

The more serious concern is that for missile motions larger than those measured at HETF-1, the missile suspension can behave quite differently. Between the small and benign seismic motion regimes, the suspension overcomes the friction between the suspension cables and cable guides. The random break- ing and locking of these friction elements would cause the rest position of the missile to walk with time. In turn, guidance system performance that re- lies on a stable missile rest position over a few bias cycles would be degrad- ed.

It is expected that over a band 0.05 to 2.5 Hz, missile roll amplitudes for Wing V can be modeled as a Rayleigh process, when operating in a benign, event-free seismic environment. Fig. 4 depicts the expected maximum roll am- plitude computed from spectral moments based on HETF-1 measurements against a pure Rayleigh process. The differences are small. Also, the observed dis- tribution in roll amplitude based on an 8 hr observation period with the HETF-1 LF sealed and unoccupied, (Fig. 5), passes a chi-square acceptance test for a Rayleigh process. Treating these data as a Rayleigh process, the max- imum roll amplitude over a 6 min bias cycle is 1.5 s͡ec. In turn, the maximum expected value for an individual missile taken over a day is 2.1 s͡ec. Taken over 200 like missiles at a time, the maximum expected roll amplitude is 2 s͡ec for a 6 min bias cycle and 2.5 s͡ec during the course of a day. In like manner for Wing VI, one can expect a maximum roll amplitude of 6 s͡ec over 200 missiles in a 6 min time frame. While for over a day the maximum roll amplitude is 10 s͡ec, as long as the MSS does not depart from its benign seismic response characteristic and missile torquing relates to air turbu- lence as the square of the mean airflow. That the MSS would remain in its seismic regime at such levels is questioned.

4.2.10 CONCLUSIONS

In this study care has been taken to reflect missile roll for a Wing V type weapon system operating in a sealed, unoccupied launch facility. Ex- trapolation of our findings to other configurations is not without risk

The missile roll envelope for a Wing V system operating in a benign, event-free seismic environment can be modeled as a Rayleigh process centered

- 48 -

at 0.43 Hz. The roll amplitude found here, 0.6 sec, is twice that given in the PVM - 11 MSS noise model.

The benign, event-free seismic environment is only a minor contributor to missile roll motion. Missile roll motion is almost exclusively due to air circulation in the launch tube.

The MSS response now carried for a Wing V system at low motion levels is not generally applicable to the minute motions encountered in an event-free seismic environment.

Missile roll for a Wing VI facility is expected to be 2 to 4 times that found for Wing V due to the larger airflow in Wing VI LFs. The prospects of reducing azimuth error at Wing VI by implementing current azimuth limit cycle prediction schemes are poor.

Missile motion levels expected for Wing VI will lead to "walking" in the missile's rest position if the motion levels are at times of a size to overcome the MSS friction elements.

Eingenvector Components at MGS
(in/in, Radians/in) Linear

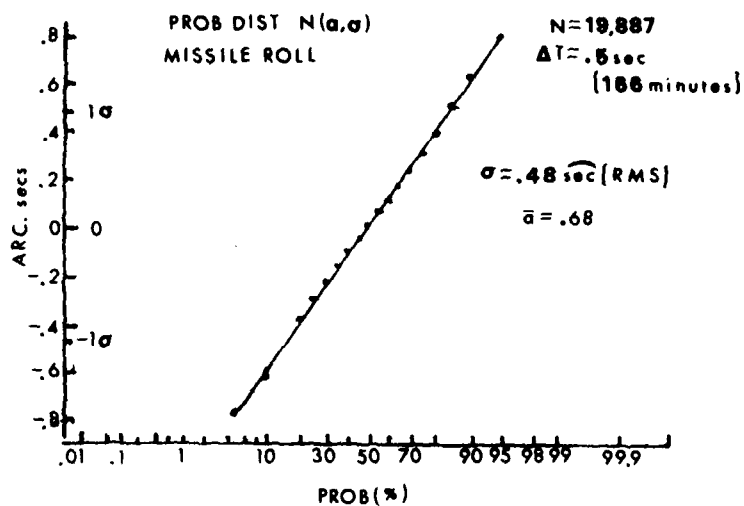|	Mode	Freq. (Hz)	Yaw	Roll	Pitch	North	West	Up	Decay Time Constant (sec)	Modal Participation (in/in)		
										v_{ix}	v_{iy}	v_{iz}
Distant Attack	1	.191	.003110	- .000186	.00170	.429	- .786	.244 -4	80	- .384	.704	.00091?
	2	.191	.00170	.545 -4	-.00310	- .785	- .429	.832 -4	80	.704	.384	.00312
	3	.293	.0320	- .000650	.0135	8.20	-19.4	.000441	80	.0319	-.0753	.827 -4
	4	.293	.0136	.000265	-.0321	-19.5	- 8.24	.00109	80	-.0750	-.0317	.000203
	5	.422	.00129	-1.00	-.00129	.191	- .191	- .240 -7	50	.688 -4	-.687 -4	-.647 -10
	6	.975	.134 -4	.315 -10	-.134 -4	-.00532	- .00532	-1.00	2	.107 -4	.108 -4	-1.011
	7	5.00	- .0146	- .000233	-.0111	-7.16	9.40	- .0163	1	.000284	-.000373	- .775 -6
	8	5.00	- .0111	.314 -4	.0146	9.40	7.16	- .121	1	-.000373	-.000284	- .574 -5
	9	9.53	- .650 -5	- .145 -11	.650 -5	-.00656	.000656	- .629	1	.175 -4	.175 -4	-.0168
	10	27.3	- .00270	-1.00	-.00270	- .610	.610	.188 -11	1	-.317 -7	.317 -7	.459 -15
	11	33.1	.00286	.256 -8	.00286	.646	.646	-.000199	.5	.119 -4	.119 -4	- .641 -5
	12	33.2	.00286	- .000759	.00286	.646	.646	.422 -9	.5	.119 -4	-.119 -4	- .460 -10

Fig. 1 Wing V Model

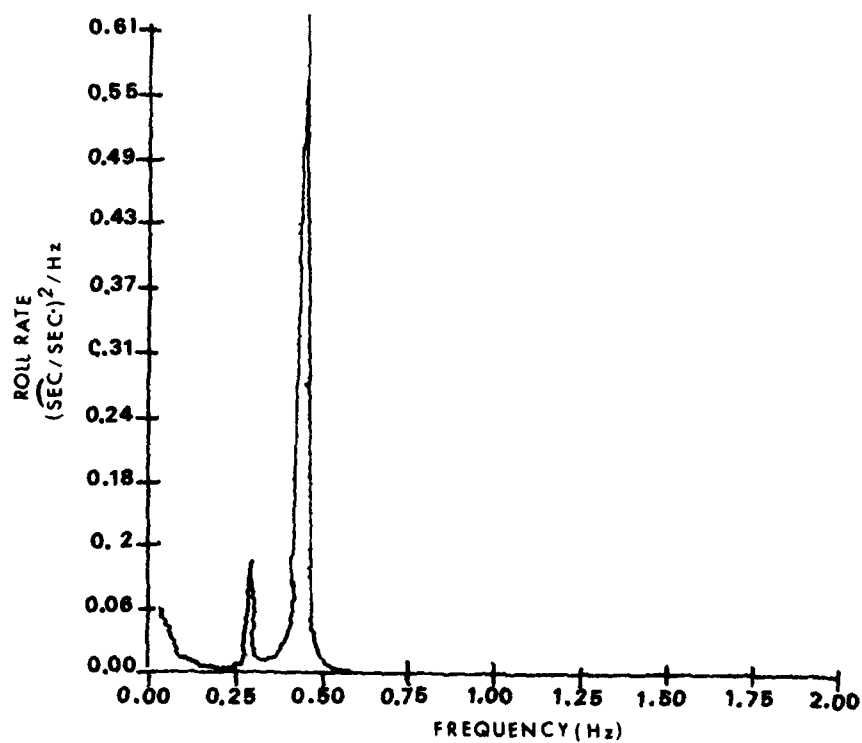Fig 2 —HETF Missile Distribution in Roll Over 166 min Benign Environment
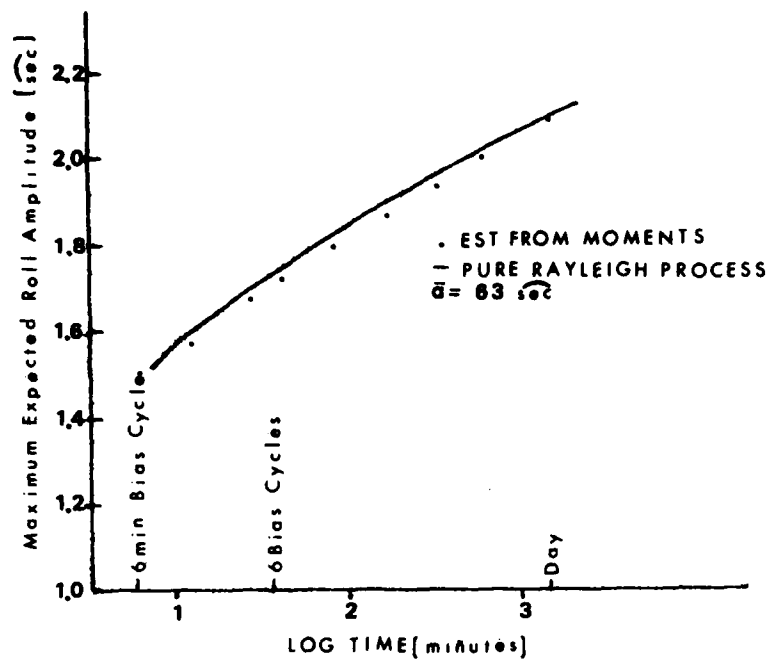

Fig 3 —A Spectral Estimate for Missile Roll Rate

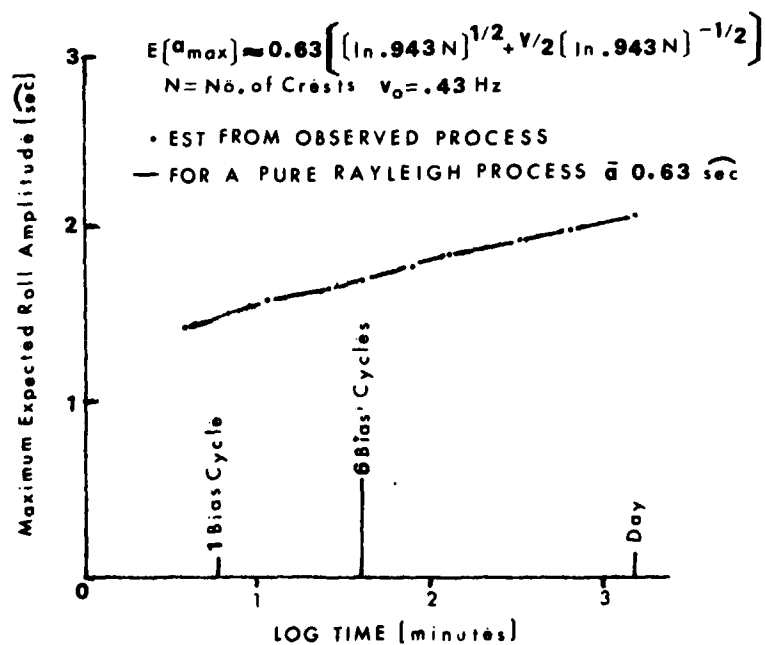FIG 4 - Expected Maximum Roll Amplitude vs a Rayleigh Process

FIG 5 - Distribution in Roll Maxima Fitted to a Rayleigh Distribution

REFERENCES

1. Crowley, F., and Hartnett, E. (1978) Roll Attributes of a Minuteman Wing V Missile In A Benign Prelaunch, Seismic Environment, AFGL-TR-28-0016.

2. Hume, R. (1975) Subject: Documentation of Gyrocompass Analysis, TRW Interoffice Correspondence.

3. Bath, M. (1973) Introduction to Seismology, John Wiley & Sons, New York.

4. Autonetics Report 76AN614868, Enclosure (1) (1976) Azimuth Limit Cycle Reduction.

5. Crowley, F., and Ossing, H. (1970) Earth Environmental Noise Fields, AFCRL-70-0460, Air Force Surveys in Geophysics No. 239.

6. Hinich, M., and Clay, C. (1968) The Application of the discrete Fourier transform in the estimation of power spectra, coherence, and bispectra of geophysical data, Reviews of Geophysics 6:347 - 363.

7. Udwadia, F., and Trifunac, M. (1974) Characterization of response spectra through the statistics of oscillator response, B.S.S.A. 64:205 - 219.

8. Frantti, G. (1965) Investigation of Short Period Seismic Noise in Major Physiographic Environments of Continental United States, AFCRL-65-406.

9. Aki, K. (1957) Space and time spectra of stationary stochastic waves with special reference to microtremors, Bul Earthq. Res. Inst. 35:416-456.

10. Penzien, J., and Watabe, M. (1975) Characteristics of 3-dimensional earthquake ground motions, Inst. J. Earthq. Engng. Struct. Dyn. 4:365-373.

11. Thomson, W., et al. (1974) A numerical study of damping, Inst. J. Earthq. Engng. Struct. Dyn. 3:97-103.

12. Boeing Report D2-26416-1 (1974) Wing F Upgrade Silo Program, Missile Suspension System, Small Motion Test Evaluation.

13. Hartnett, E. (1977) A Simulation Study of a Twelve Degree of Freedom System, AFGL-TR-77-0061.

14. Statonovich, R. (1963) Topics in the Theory of Random Noise, Gordon and Breach, New York.

15. Sage, A., and Melsa, J. (1971) System Identification, Academic Press, New York.

16. Crowley, F., and Ossing, H. (1973) A Motion Study of the Frank J. Seiler Research Laboratory Test Facility, AFCRL-TR-0417.

REFERENCES

17. Shearer, J., and Anthony, D. (1978) Long Period Azimuthal Motion Effects on Minuteman Upgrade Missiles, in press.

18. Perry, E. (1976) Very Small Motion Vertical Response of Upgrade MSS, TRW Technical Note dated 31 August 1976.

19. Kuenzler, H., et al (1975) Modifications and Additions to the Geokinetic Data Acquition System, AFCRL-TR-75-0434.

ABBREVIATIONS, ACRONYMS AND SYMBOLS

AAMS   -   Automated Azimuth Measuring Set

AFGL   -   Air Force Geophysics Laboratory

AGMC   -   Aerospace Guidance and Metrology Center

AITL   -   Advanced Inertial Test Laboratory

ALS   -   Azimuth Laying Set

BMO   -   Ballistic Missile Office

CEP   -   Circular Error Probable

CIGIF   -   Central Inertial Guidance Test Facility

GCA   -   Gyrocompass Assembly

GDAS   -   Geokinetic Data Acquisition System

HEFT   -   Hill Engineering Test Facility

IPD   -   Inertial Performance Data

LCC   -   Launch Control Center

LF   -   Launch Facility

MGS   -   Missile Guidance Set

MSS   -   Missile Suspension System

PPR   -   Payload Preparation Room

SADAS   -   Stand Alone Data Acquisition System

SAM   -   Seismic Activity Monitor

SAMSO   -   Space and Missile Systems Office

SD   -   Space Division

SERDEX -   Serial Data Exchange

SLC   -   Space Launch Complex

STM   -   Special Test Module

STA   -   Space Transportation Shuttle

TGG   -   Third Generation Gyro